GAN-Enhanced Radial Basis Function Networks for Improved Landslide Susceptibility Mapping

Chyntia Raras Ajeng Widiawati[1], Ika Maulita[2], Yuli Purwati[3], Arif Mu'amar Wahid[4,*]

[1]*Information Technology Department, Universitas Amikom Purwokerto, Banyumas 53127, Indonesia*

[2]*Physics Department, Universitas Jenderal Soedirman, Banyumas 53123, Indonesia*

[3,4]*Informatics Department, Universitas Amikom Purwokerto, Banyumas 53127, Indonesia*

[4]*Division of Electrical, Information and Communication Engineering, Graduate School of Natural Science and Technology, Kanazawa University, Kanazawa 920-1192, Japan*

(Received: July 15, 2025; Revised: September 10, 2025; Accepted: December 12, 2025; Available online: January 14, 2026)

Abstract

This study proposes a GAN-augmented Radial Basis Function Network (RBFN) framework to address severe data imbalance in landslide susceptibility modeling for Malang Regency, East Java. The idea is to rehabilitate imbalance-sensitive neural networks that normally collapse under a 1:10 landslide–non-landslide ratio by combining rigorous spatial preprocessing, feature engineering, and generative augmentation. A geocoded inventory of 81 landslides and 810 non-landslide locations was constructed using a three-tier geocoding scheme and nine predictors (elevation, slope, NDVI, rainfall, geology, soil, distance to faults, distance to rivers, and river density). The objectives are to (i) quantify model degradation under imbalance, (ii) rebalance the minority class using GAN-generated samples, and (iii) optimize and benchmark RBFN against Random Forest (RF) and K-Nearest Neighbors (KNN). Baseline experiments on the imbalanced dataset show RF performing robustly (F1-Score = 0.9677, Recall = 0.9375, AUC = 0.9904), while KNN degrades (F1-Score = 0.72) and RBFN fails completely (F1-Score = 0.00, Recall = 0.00). A GAN trained on 65 landslide samples produced 582 synthetic events, yielding a balanced 1:1 training set. After augmentation and grid-search tuning (150 hidden neurons, β = 1.5, 150 epochs), the RBFN achieved Accuracy = 0.9888, F1-Score = 0.9333, Recall = 0.8750, and AUC = 0.9804 on an untouched imbalanced test set. The main contribution and novelty lie in demonstrating that GAN-based augmentation can transform RBFN into a high-performing classifier competitive with RF, providing a practical pathway to improve landslide susceptibility mapping under extreme class imbalance.

Keywords: Landslide Susceptibility, Generative Adversarial Network (GAN), RBFN, Data Imbalance, Geospatial Machine Learning

1. Introduction

Landslides are among the most destructive geological hazards in Indonesia [1]. The nation's position on the Pacific Ring of Fire produces tectonic activity, steep volcanic terrain, and unstable slopes [2]. Combined with a tropical climate delivering intense seasonal rainfall, these conditions frequently trigger catastrophic landslides that destroy infrastructure, disrupt economies, and claim many lives [3]. According to the National Disaster Management Agency (BNPB), 634 landslide events were recorded in 2022 alone [4], with most occurring during the rainy season as soil saturation weakens slope stability. Landslide occurrence results from a complex interplay of natural and human-induced factors [5], [6]. Geological structures such as weathered volcanic deposits or weak sedimentary layers contribute to inherent instability, while deforestation and unplanned development exacerbate slope failures by removing vegetation cover and altering drainage patterns [7], [3].

The consequences extend beyond immediate physical loss to long-term socioeconomic disruption [8]. Malang Regency, East Java—characterized by volcanic topography, dense population, and intensive land use—was therefore

*Corresponding author: Arif Mu'amar Wahid (arif@amikompurwokerto.ac.id)
DOI: https://doi.org/10.47738/jads.v7i1.1035

selected as a representative case study [1]. A key technical challenge in landslide susceptibility modeling is the severe class imbalance of available data.

Landslide events (minority class) are far fewer than stable, non-landslide samples (majority class), leading to biased models that yield deceptively high accuracy yet fail to predict true landslides [9], [10]. Such imbalance causes false negatives, undermining hazard maps and early-warning systems. To address this issue, data augmentation methods such as SMOTE have been applied but often fail to capture the complex non-linear relationships of geospatial data. In contrast, GAN can model underlying data distributions to generate realistic samples. This study integrates GAN-based augmentation with a RBFN, a non-linear model that is powerful yet sensitive to imbalance [11], [12]. The proposed framework aims to (i) evaluate model degradation under imbalance, (ii) employ GAN to rebalance data, (iii) optimize RBFN performance, and (iv) compare results using Recall, F1-Score, and AUC metrics.

2. Literature Review

2.1. Landslide Susceptibility Modeling

Landslide susceptibility modeling seeks to identify and map areas with a high likelihood of slope failure, forming a critical foundation for hazard mitigation and spatial planning [13]. The accuracy of such models depends on selecting and analyzing conditioning factors that influence slope stability. These factors are generally grouped into topographic, geological, hydrological, and land-use variables. Topographic parameters, including slope angle, elevation, and aspect—commonly derived from Digital Elevation Models (DEMs)—govern gravitational forces acting on slopes [14]. Geological factors such as lithology and soil type determine the inherent strength of materials, while hydrological parameters like rainfall intensity, duration, and proximity to rivers affect soil saturation and pore pressure, the main triggers of failure [7]. Land-use and vegetation characteristics, often measured using the Normalized Difference Vegetation Index (NDVI), can either reinforce or weaken slope stability, with deforestation and poor land management significantly increasing risk [3]. As emphasized in the literature, selecting regionally relevant factors based on their physical significance ensures the resulting susceptibility model is both reliable and applicable for local hazard assessment [15].

2.2. Machine Learning in Landslide Prediction

The use of machine learning has greatly advanced landslide susceptibility prediction by capturing complex, non-linear relationships among conditioning factors. Various models have been applied, with ensemble methods such as RF gaining prominence for their accuracy and robustness through the aggregation of multiple decision trees. Studies by [6] and [16] confirmed RF's effectiveness in handling high-dimensional data and its resilience to class imbalance [17], [18]. Simpler models like KNN also appear frequently, classifying samples based on the majority class of their nearest neighbors using Euclidean distance, as expressed in (1).

$$d(p,q) = \sum (p_i - q_i)^2 \quad (1)$$

d(p, q): The Euclidean distance between two data points, p and q. p_i and q_i: The value of the i-th feature for points p and q, respectively. Another powerful model is Support Vector Machines (SVM), which work by finding an optimal hyperplane to separate classes, defined by the equation (2)

$$w \cdot x - b = 0 \quad (2)$$

W: The weight vector, which is perpendicular to the hyperplane and controls its orientation. X: The input feature vector for a single data point. B: The bias or intercept term, which shifts the hyperplane.

While these models have proven useful, they can have limitations in capturing the most intricate patterns present in complex geospatial datasets. To address the limitations of conventional models, researchers have increasingly turned to neural network architectures capable of modeling more complex phenomena. The RBFN is one such model that has shown significant promise in geospatial modeling. Unlike traditional multi-layer perceptrons, RBFNs utilize radial basis functions as activation functions [19]. A common choice is the Gaussian RBF, as shown in formula (3).

$$\phi(r) = e - (\epsilon r)^2 \quad (3)$$

 ISSN 2723-6471

ϕ(r) : The output of the radial basis function, which decreases as the distance r increases. e : Euler's number (the base of the natural logarithm). r : The distance from the input to a central point. ε : The shape parameter that controls the "width" of the function. The network's output is then a weighted sum of these functions, making it particularly adept at function approximation and pattern recognition in high-dimensional spaces (4).

$$y(x) = i = 1 \sum Nwi\phi(\| x - ci \|) \quad (4)$$

y(x) : The final predicted output of the RBFN for a given input x. w_i : The weight associated with the i-th neuron. Φ : The radial basis function (the Gaussian function). $\|x - c_i\|$: The Euclidean distance between the input vector x and the center vector c_i of the i-th neuron. N : The total number of neurons in the hidden layer.

Research [11] emphasized the strength of Radial Basis Function Networks (RBFNs) in capturing complex, non-linear interactions among landslide conditioning factors such as slope, rainfall, and geology, making them suitable for susceptibility mapping. Recent studies have also explored deep learning for landslide analysis, with [20] and [8] demonstrating its effectiveness in delineating landslide boundaries from remote sensing data. These advancements highlight the potential of neural networks like RBFN to deliver more accurate predictions. Nevertheless, the performance of all such models ultimately depends on data quality and balance, which remain critical challenges in landslide inventory modeling.

2.3. The Data Imbalance Problem

Despite advances in machine learning, predictive performance in natural hazard modeling remains constrained by the persistent challenge of data imbalance [21], [22]. In landslide prediction, the minority class (landslide events) is inherently rare compared to the vast areas of stable terrain. As noted by [9], even frequent landslides in Indonesia occupy only a small portion of spatial datasets, causing standard algorithms—optimized to minimize total error—to become biased toward the majority class. Consequently, models may achieve high overall accuracy by predicting “no landslide” for most points, while entirely missing true events. This results in dangerous false negatives, where hazardous areas are incorrectly labeled as safe [23]. As [10] highlighted, such imbalance produces models with high accuracy but low real-world utility. To address this, evaluation should prioritize metrics sensitive to minority detection. Recall, which measures the proportion of correctly identified landslides, and Precision, which quantifies prediction accuracy, are best balanced through the F1-Score—making it the key metric for assessing hazard models trained on imbalanced data.

2.4. Generative Adversarial Networks (GANs) for Data Augmentation

To overcome data imbalance, recent studies have increasingly adopted advanced augmentation methods, with GAN emerging as a state-of-the-art solution. A GAN consists of two neural networks—a Generator that learns the data distribution to create synthetic samples and a Discriminator that distinguishes real from fake data. Through their adversarial training, the Generator progressively produces synthetic data that become statistically indistinguishable from real samples, effectively enriching the minority class. GANs have demonstrated strong performance in generating realistic tabular and geospatial data, making them highly relevant for landslide modeling. As shown by [10], GAN-based augmentation can rebalance landslide datasets, enabling models to better learn minority-class patterns, improve predictive accuracy, and reduce false negatives. This confirms GANs’ potential to address data scarcity and imbalance in natural hazard research. However, few studies have explored GAN integration with specific neural classifiers such as the RBFN. Most prior works relied on oversampling techniques like SMOTE [16] or CTGAN, which fail to capture complex non-linear relationships among geospatial factors. Thus, this study fills a notable gap by developing and validating a GAN-RBFN framework designed to enhance imbalance-sensitive models and advance the reliability of landslide susceptibility mapping.

 ISSN 2723-6471

3. Method

Figure 1 summarizes the methodological workflow of this study, from spatial data preparation and geocoding through feature extraction and exploratory data analysis to baseline and GAN-augmented machine learning modeling, followed by evaluation and validation.

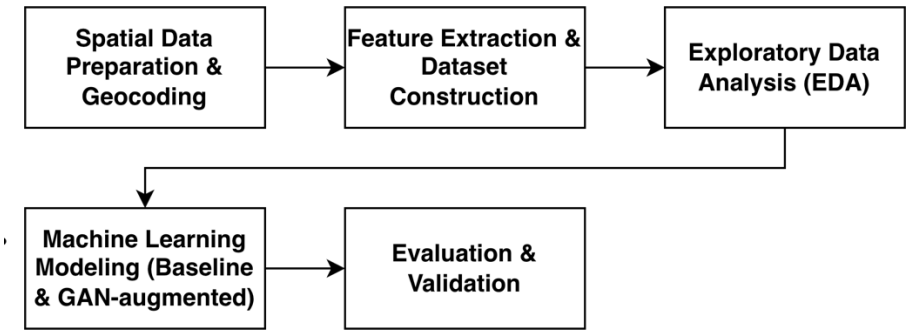

Figure 1. Research Method Flowchart

3.1. Spatial Data Preparation and Pre-processing

The study began by converting a text-based landslide inventory from BPBD Malang Regency into a geocoded dataset for spatial analysis. The original CSV contained only location names—Dusun, Desa, and Kecamatan—so a geocoding workflow was required to obtain coordinates. A Python script queried the Nominatim API using concatenated location strings with a one-second delay, achieving a 12.27% success rate due to inconsistent entries. A three-tiered strategy was then applied: full query (hamlet–village–sub-district), simplified query (without hamlet), and broad query (sub-district only), improving accuracy to 99.39%. Remaining errors were manually corrected for typographical issues such as “Wonosarri” to “Wonosari” and “Sumawe” to “Sumbermanjing Wetan.” After a final cleanup, invalid rows without coordinates were removed, producing a complete and spatially valid dataset ready for feature extraction.

For clarity and reproducibility, the tiered geocoding workflow can be expressed directly in mathematical form as follows. First, we represent the landslide records as:

$$D = \{(d_i, v_i, k_i) \mid i = 1, \dots, n\} \tag{5}$$

d_i, v_i, and k_i denote the Dusun, Desa, and Kecamatan of record (i), respectively. Let:

$$G: Q \to R^2 \times A \cup \{\emptyset\} \tag{6}$$

be a geocoding function that maps a textual query $q \in Q$ either to a tuple (φ, λ, a), consisting of latitude (φ), longitude (λ), and formatted address ($a \in A$), or to ($\emptyset$) if no valid location is found. For each record (i), we construct up to three hierarchical queries:

$$q_i^{(1)} = \text{"}d_i, v_i, k_i, \text{ Kabupaten Malang, Indonesia"}$$

$$q_i^{(2)} = \text{"}v_i, k_i, \text{ Kabupaten Malang, Indonesia"} \tag{7}$$

$$q_i^{(3)} = \text{"}k_i, \text{ Kabupaten Malang, Indonesia}$$

The coordinates assigned to record (i) are obtained by:

$$(\varphi_i, \lambda_i, a_i) = G!\left(q_i^{(1)}\right) \tag{8}$$

and, if this first query fails, by successively falling back to coarser queries:

 ISSN 2723-6471

$$\text{if } G\left(q_i^{(1)}\right) = \emptyset \text{ then } (\varphi_i, \lambda_i, a_i) = G\left(q_i^{(2)}\right)$$

$$\text{if } G\left(q_i^{(1)}\right) = \emptyset \text{ and } G\left(q_i^{(2)}\right) = \emptyset \text{ then } (\varphi_i, \lambda_i, a_i) = G\left(q_i^{(3)}\right) \tag{9}$$

$$\text{if } G\left(q_i^{(1)}\right) = \emptyset \text{ and } G\left(q_i^{(2)}\right) = \emptyset \text{ and } G\left(q_i^{(3)}\right) = \emptyset \text{ then record } i \text{ is "Not Found"}$$

Finally, we define the index sets of successfully geocoded and failed records as:

$$I = \{i | (\varphi_i, \lambda_i, a_i) \neq \emptyset\}, \qquad N = \{i | (\varphi_i, \lambda_i, a_i) = \emptyset\} \tag{10}$$

3.2. Feature Extraction and Dataset Construction

This stage converted the cleaned, geocoded landslide locations into a feature-rich dataset for machine learning. Two workflows were carried out: enriching landslide points with relevant environmental factors and generating non-landslide points with identical features. Nine predictors were selected based on established relevance: elevation and slope from DEMNAS (BIG), vegetation density (NDVI) from Landsat 8 (USGS), rainfall from CHIRPS, geology from the national geological map, soil type from the FAO DSMW, and distance-based variables—faults, rivers, and river density—from RBI and ESDM maps. Raster variables were sampled directly at each coordinate, while categorical features were encoded using one-hot encoding. All coordinates were reprojected to UTM Zone 49S for distance calculations. Non-landslide samples were generated by randomly selecting pixels with slopes below 3.5%, representing stable terrain, maintaining a 10:1 ratio between non-landslide and landslide points. Both datasets were combined into a single labeled file, where status values of 1 and 0 indicated landslide and non-landslide points, forming the final dataset for analysis and model training. For clarity and reproducibility, the feature-extraction can be expressed mathematically as follows. We consider geographic coordinates (x = (lon,lat) $\in \Omega \subset R^2$). The set of mapped landslide locations is:

$$L = \{x_i^+ \mid i = 1, \ldots, n_+\} \subset \Omega. \tag{11}$$

The input rasters are represented as functions:

$$E_{\text{elev}}: \Omega \to R, \quad S_{\text{slope}}: \Omega \to R, \quad N_{\text{NDVI}}: \Omega \to R, \quad R_{\text{rain}}: \Omega \to R, \quad G_{\text{geo}}: \Omega \to \mathcal{G}, \quad S_{\text{soil}}: \Omega \to \mathcal{S} \tag{12}$$

($\mathcal{G}$) and ($\mathcal{S}$) are the sets of geology and soil classes, respectively. Let ($A_{\text{Malang}} \subset \Omega$) denote the administrative boundary of Kabupaten Malang. In the projected (metric) coordinate system we use $T: \Omega \to R^{\mathbb{2}}$ to denote the reprojection from $CRS_{GEO} = EPSG: 4326$ to $CRS_{GEO} = EPSG: 32749$.

3.3. Exploratory Data Analysis

Before model development, an Exploratory Data Analysis (EDA) was conducted to examine dataset quality and identify distinguishing features between landslide and non-landslide locations. The process consisted of two phases. The first analyzed only landslide points, focusing on data cleaning, descriptive statistics, and visualization. Key numeric fields—such as elevation, slope, NDVI, rainfall, and distance metrics—were converted to numeric format, with missing or invalid values removed. Summary statistics (mean, median, standard deviation) and frequency counts for categorical features (Kecamatan, geology, soil type) were generated to identify dominant patterns. Visualizations, including histograms, bar charts, and correlation heatmaps, illustrated variable distributions and relationships among predictors. The second phase compared landslide and non-landslide points within the imbalanced dataset. After similar cleaning, binary class labels were mapped as “Longsor” and “Non-Longsor.” Comparative statistics and visualizations—box plots for numerical features and grouped bar charts for categorical ones—highlighted key differences, such as higher slopes and elevations in landslide areas. This phase clarified how environmental factors contribute to susceptibility and informed subsequent modeling strategies. While the EDA revealed meaningful contrasts between classes, it did not include advanced analyses such as feature importance or multicollinearity testing, which are noted as limitations for future work.

3.4. Machine Learning Modeling

This stage formed the core experimental phase, where predictive models were developed, trained, and optimized to identify landslide susceptibility patterns. Baseline performance was first established using the raw imbalanced dataset to measure classification difficulty and provide a benchmark for later improvements through GAN augmentation. The dataset was preprocessed by converting numeric fields (elevation, slope, rainfall, distance metrics) to numeric types and encoding categorical variables (geology, soil type) via one-hot encoding. Data were split into training (80%) and testing (20%) sets using stratified sampling to maintain the 10:1 imbalance, then standardized with Scikit-learn's StandardScaler to normalize feature ranges. Three baseline models were trained: Random Forest (ensemble-based), K-Nearest Neighbors (instance-based), and Radial Basis Function Network (neural network-based). To mitigate imbalance, a GAN with dense layers, LeakyReLU activation, and Dropout regularization was trained for 15,000 epochs on minority samples. The trained Generator produced synthetic landslide data, balancing the classes at a 1:1 ratio. Random Forest and KNN were retrained, while the RBFN underwent grid search optimization for hidden neurons, beta, and epochs, achieving the best configuration based on F1-Score. GAN training required about 25 minutes and RBFN tuning 40 minutes on a Colab T4 GPU, both feasible within standard research resources.

3.5. Evaluation and Validation

The final stage of the methodology was dedicated to the quantitative evaluation and validation of all trained models. Performance was assessed on the held-out test set, which retained the original 10:1 class imbalance in order to approximate real-world conditions. A suite of commonly used metrics was employed: Accuracy, Precision, Recall, F1-Score, and the Area Under the ROC Curve (AUC). Although Accuracy was calculated, it was not considered a primary metric due to its sensitivity to imbalance. Instead, Recall and F1-Score were emphasized as key indicators: Recall measures the model's ability to correctly identify true landslide events, while the F1-Score balances Recall and Precision to provide a robust measure of minority-class performance. AUC was also included to provide a threshold-independent measure of overall discriminative power.

Each trained model was evaluated on the test set using the same metrics to ensure comparability between baseline (imbalanced) and augmented (GAN-balanced) models. To avoid bias, stratified train–test splitting was used, and no test data were included during model training or augmentation. Several visualization techniques were applied to present model performance in a clear and interpretable manner: a) Performance tables, reporting metrics side-by-side for all models; b) Combined ROC curve plots, illustrating classification trade-offs across thresholds; c) Bar charts comparing Recall and F1-Score between models; and d) Confusion matrices for each model, showing counts of true positives, true negatives, false positives, and false negatives. Together, these metrics and visualizations provided a systematic and replicable framework for evaluating model performance and validating the effectiveness of the GAN-based augmentation strategy.

4. Results and Discussion

4.1. EDA Results

The EDA was conducted in two phases: first, an analysis of landslide-only locations to characterize their intrinsic properties, and second, a comparative analysis between landslide and non-landslide points to identify distinguishing factors. Descriptive statistics for the 81 landslide locations reveal a distinct environmental profile. On average, events occurred at an elevation of 503.6 m with a mean slope of 11.52%. The sites ranged from 30.6 m to 1066.2 m in elevation and from 1.24% to 48.67% in slope, while average annual rainfall was 2142.6 mm. Frequency analysis of categorical variables showed that the Tengger Volcanic Formation (Qvtm1) was the most common geological unit, and Inceptisols (I) and Andosols (Je) were the most common soil types. Administratively, Tirtoyudo sub-district recorded the highest number of events.

Comparison with 810 non-landslide points highlights slope as the most distinctive variable: landslide sites averaged 11.52% slope, compared with only 2.24% for non-landslides. Elevation also differed, with landslide sites averaging 503.6 m versus 430.5 m. NDVI values were slightly higher in stable locations (0.30 vs. 0.25), consistent with denser vegetation cover providing stabilizing effects. Rainfall and distance to faults showed less clear separation. Crosstabulation of categorical features indicated that some units, such as Qpkb, were frequent across the study area but

ISSN 2723-6471

not proportionally overrepresented in landslide cases, suggesting geology alone is not deterministic. The statistical contrasts were illustrated through multiple visualizations. Histograms of slope and elevation (figure 2) showed clustering of landslides at mid-elevations (400–600 m) and moderate slopes, with fewer cases on extreme slopes.

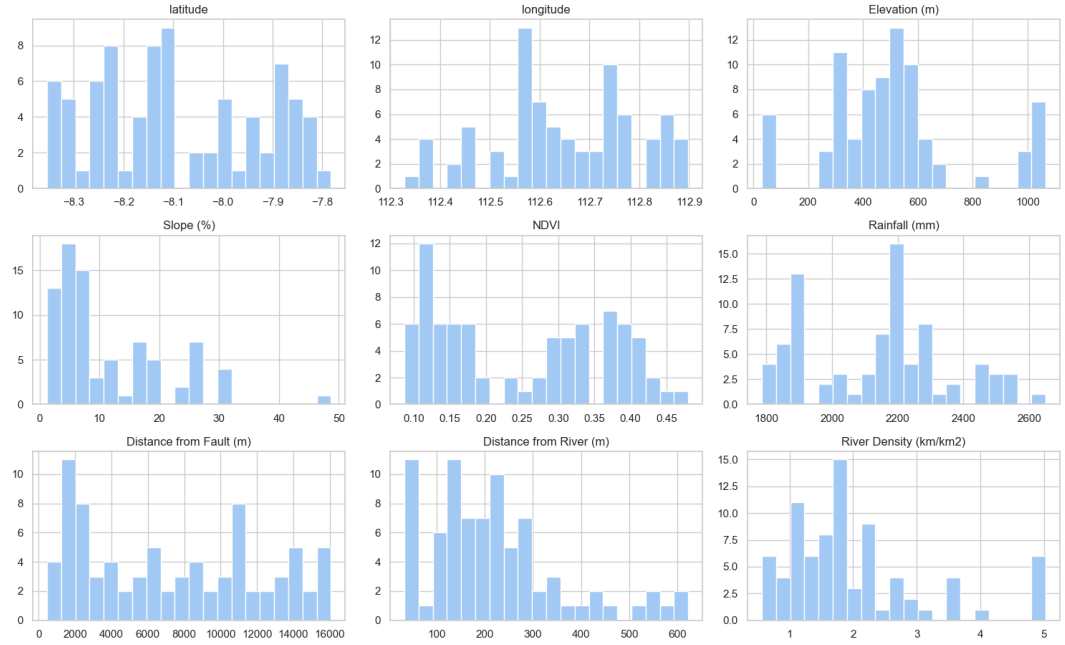

Figure 2. Distribution of Numerical Parameters for Landslide Locations

Box plots (figure 3) confirmed slope as a strong discriminator: the interquartile range for landslide sites was well above that of non-landslides. Elevation also showed a higher distribution for landslide cases.

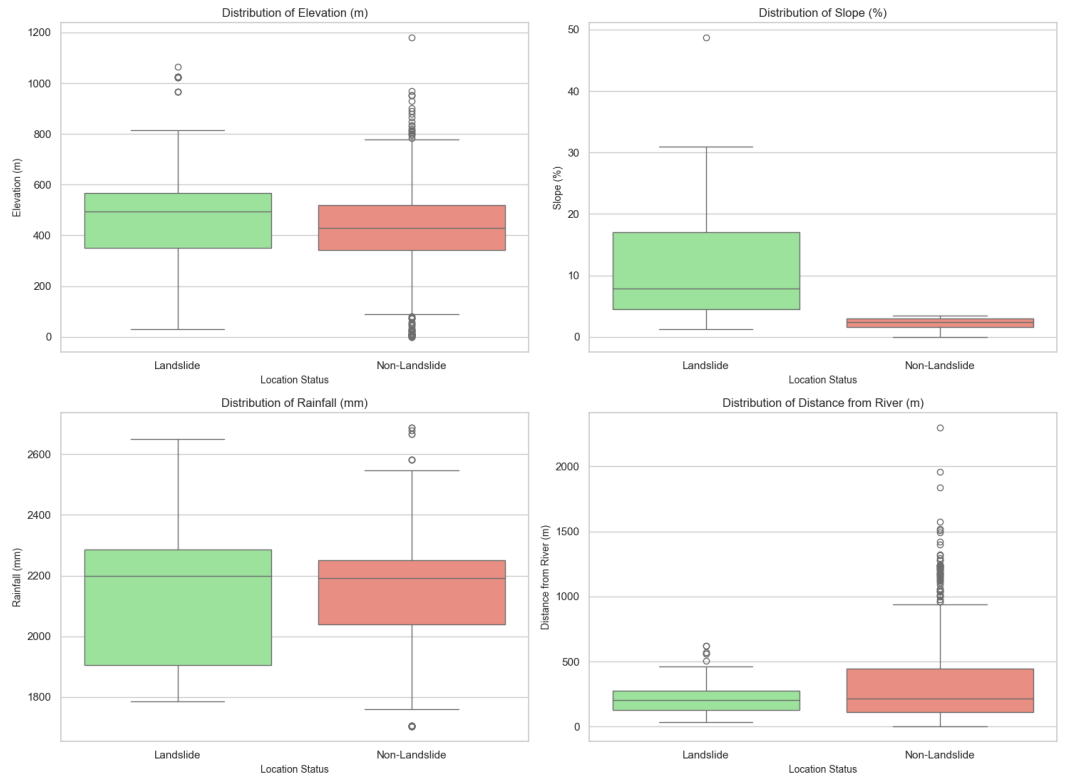

Figure 3. Comparison of Numerical Parameter Distributions

Grouped bar charts (figure 4) compared categorical frequencies, showing Andosols (Je) and Inceptisols (I) as prevalent soil types across both classes.

ISSN 2723-6471

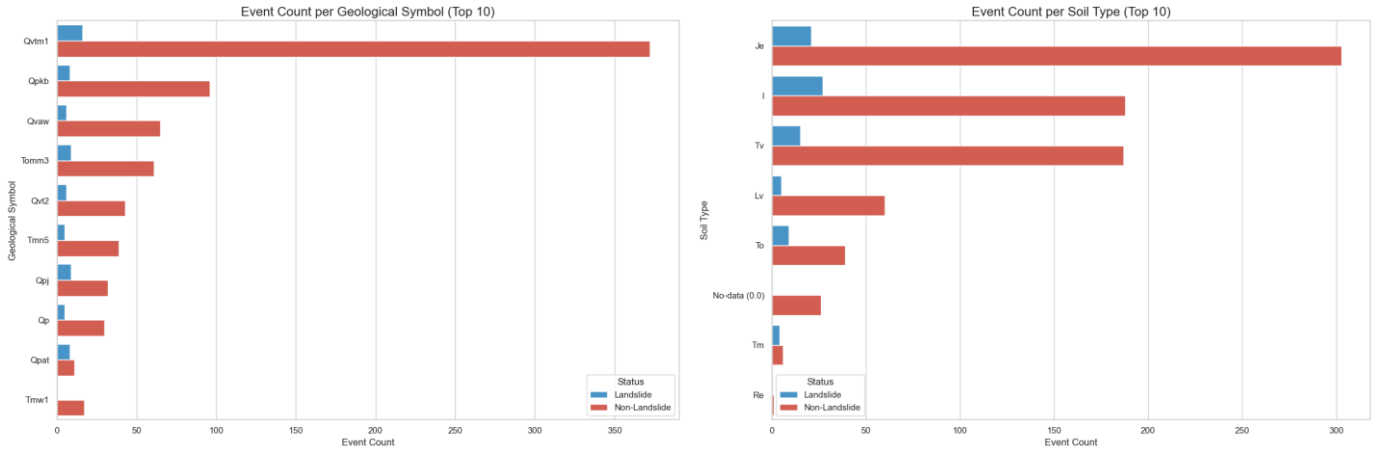

Figure 4. Bar Charts of Categorical Features

The correlation heatmap (figure 5) suggested weak linear correlations, with elevation (0.12) and slope (0.11) positively associated with landslides and distance to rivers negatively associated (-0.10). These weak values indicate that the relationships are likely non-linear, underscoring the appropriateness of advanced machine learning approaches. While the EDA revealed several key differentiators, it did not include formal feature importance measures or multicollinearity checks (e.g., Variance Inflation Factor). This omission is acknowledged as a limitation, and future work should incorporate such tests to better quantify predictor contributions and dependencies.

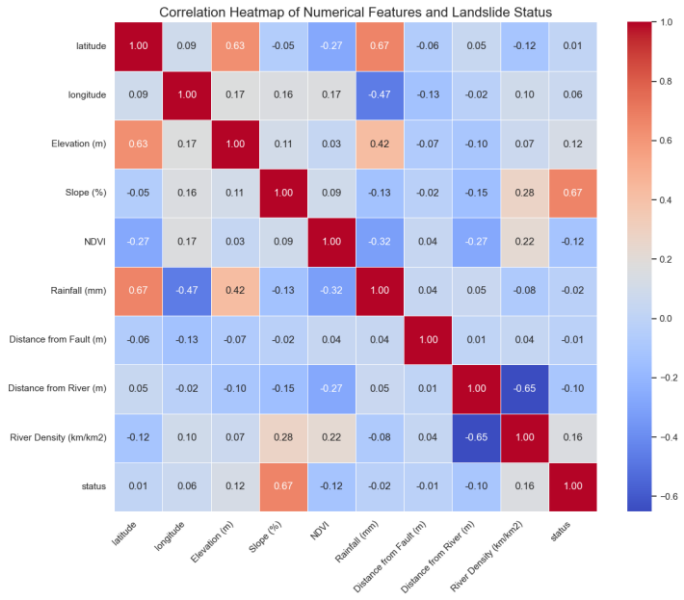

Figure 5. Correlation Heatmaps

4.2. Baseline Model Performance on Imbalanced Data

To establish a performance benchmark, three baseline models RF, KNN and a RBFN—were trained on the original, highly imbalanced dataset (1:10 ratio). The evaluation, conducted on the unseen test set, revealed the severe impact of this data imbalance on model performance, as summarized in the table1. The Random Forest model demonstrated remarkable robustness, achieving a near-perfect F1-Score of 0.9677 and a high Recall of 0.9375 for the landslide class. In contrast, the KNN model struggled significantly, managing a much lower Recall of 0.5625, indicating it failed to identify nearly half of the actual landslide events. The RBFN, being the most sensitive to the data distribution, exhibited a complete predictive failure for the minority class, resulting in a Recall and F1-Score of 0.00. This outcome confirms that without intervention, the RBFN developed a severe bias towards the majority (non-landslide) class, learning that the optimal strategy to minimize overall error was to ignore the minority class entirely, rendering it unusable for practical hazard detection.

Table 1. Performance of Baseline Models Trained on the Imbalanced Dataset

Model	Accuracy	Precision (Landslide)	Recall (Landslide)	F1-Score (Landslide)	AUC-ROC
Random Forest	0.9944	1	0.9375	0.9677	0.9904
K-Nearest Neighbors	0.9609	1	0.5625	0.72	0.9544
RBF Network	0.9106	0	0	0	0.8294

4.3. GAN Training and Data Augmentation

Following the baseline evaluation, a GAN was implemented to address the class disparity. The GAN was trained exclusively on the 65 landslide samples from the training set in an adversarial process over 15,000 epochs. During this training, the Generator network learned to create synthetic data, while a competing Discriminator network learned to distinguish real from synthetic data. The process was deemed successful as the loss functions for both networks stabilized, indicating the Generator had become proficient at producing realistic synthetic data that could consistently fool the Discriminator. The trained generator was then used to create 582 synthetic landslide samples. This number was calculated to precisely match the 647 non-landslide samples in the training set, thereby transforming the original imbalanced data into a numerically balanced 1:1 dataset for retraining the models. The successful rebalancing of the training data was visually confirmed by comparing the class distribution before and after the augmentation process.

4.4. Performance of Models with GAN Augmentation

With the training data balanced by the GAN-generated samples, all models were retrained and re-evaluated on the same, untouched test set. The Random Forest and KNN models showed no significant change in performance. This result was expected for the already robust Random Forest, and it suggests that the simpler, distance-based logic of KNN did not gain the same level of nuanced pattern recognition from the synthetic data as a more complex model might. Crucially, this reinforces that the augmented data did not degrade their predictive power.

The most significant result of this study is the dramatic turnaround of the RBFN model. After being retrained on the augmented data and undergoing a systematic hyperparameter tuning process, the optimized RBFN achieved an F1-Score of 0.9333 and a Recall of 0.8750 (see table 2). This represents an increase from zero, transforming the model from a completely non-functional state—where it had learned to simply ignore the minority class to achieve high accuracy—into a highly effective and reliable predictor. This transformation was a two-stage process: first, the GAN provided the thousands of realistic minority-class examples necessary for the RBFN to even begin learning the complex patterns of a landslide event. Second, the hyperparameter tuning process refined the model's architecture, allowing it to make the most efficient use of this new, richer dataset. The optimal parameters identified through the tuning process were 150 hidden neurons, a beta value of 1.5, and 150 training epochs. This successful optimization elevated the RBFN's performance to a level highly competitive with the robust Random Forest model, conclusively demonstrating that the proposed GAN-based augmentation strategy is profoundly effective at rescuing and empowering models that are otherwise vulnerable to severe class imbalance. The analysis of the confusion matrices for the augmented models confirmed a substantial reduction in false negatives, particularly for the RBFN.

Table 2. Model Performance After GAN Augmentation

Model	Accuracy	Precision (Landslide)	Recall (Landslide)	F1-Score (Landslide)	AUC-ROC
Random Forest (GAN)	0.9944	F1	0.9375	0.9677	0.9781
K-Nearest Neighbors (GAN)	0.9609	1	0.5625	0.72	0.9544
RBF Network (GAN - Optimized)	0.9888	1	0.875	0.9333	0.9804

4.5. The Impact of Data Imbalance

The initial baseline evaluation starkly illustrates the critical vulnerability of standard machine learning models to severe class imbalance. The performance of the KNN and, most notably, the RBFN models collapsed when trained on the 1:10 imbalanced dataset. This failure is a direct and predictable consequence of how these algorithms' learning

objective's function. Both models, in their attempt to minimize overall classification error across the entire dataset, developed a strong and ultimately debilitating bias towards the majority (non-landslide) class. For the KNN, which operates on a principle of proximity-based voting, any new data point representing a true landslide was far more likely to be geographically surrounded by the ten-times-more-numerous non-landslide neighbors in the feature space. This numerical dominance effectively drowned out the "votes" of the few true landslide neighbors, leading the model to consistently misclassify these critical events.

The RBFN's failure was even more absolute and systemic. Its learning process relies on positioning radial basis functions as centers to map the data's distribution. In a heavily skewed environment, the algorithm's optimization process was completely overwhelmed by the prevalence of non-landslide samples. The model effectively concluded that the most efficient path to achieving high accuracy was to learn a simplistic, trivial rule: always predict "non-landslide." This strategy, while mathematically sound for minimizing total error on an imbalanced dataset, resulted in a model with a deceptively high accuracy (91%) but a Recall of zero for the landslide class. This outcome epitomizes the "accuracy paradox," where a high accuracy score masks a model's complete inability to predict the event of interest. The practical implication of this is profound: a model that produces dangerously high numbers of false negatives would lead to flawed susceptibility maps and misinformed land-use policies, actively increasing community risk by incorrectly labeling hazardous areas as safe.

4.6. Discussion: Efficacy, Comparison, and Limitations

The improvement of the RBFN after augmentation can be explained by a two-stage mechanism. The first stage was data augmentation with the GAN, trained for 15,000 epochs on the minority class. This process allowed the generator to approximate the multi-dimensional distribution of landslide events and to produce diverse synthetic samples that enriched previously sparse regions of the feature space. These additional data points enabled the RBFN to establish more robust and nuanced decision boundaries. It should be noted, however, that stabilization of the GAN's loss functions was used as a practical training indicator but is not definitive proof of sample quality. Future work should incorporate qualitative assessments such as t-SNE distribution comparisons or expert validation to confirm the fidelity of generated data. The second stage was hyperparameter optimization, performed via grid search. Thirty-two configurations were evaluated, and the best results were achieved with 150 hidden neurons, a beta value of 1.5, and 150 training epochs. These parameters collectively determined the model's ability to capture the complexity introduced by the augmented dataset. A limitation of this study is the absence of an ablation analysis to separate the contributions of augmentation and tuning; further research could address this distinction by testing tuned models on the original imbalanced data.

In comparing models, Random Forest consistently delivered high performance, reflecting the robustness of ensemble learning methods that leverage bagging and feature randomness. Rather than attempting to surpass Random Forest, the value of this work lies in demonstrating the transformative effect of the GAN-RBFN pipeline. A model that initially failed under severe imbalance was elevated to a performance level approaching that of Random Forest. This suggests that augmentation strategies can rehabilitate imbalance-sensitive algorithms, enabling researchers to select models for their theoretical suitability—such as RBFN's strength in capturing non-linear patterns—while mitigating structural weaknesses.

Several limitations must be acknowledged. First, the quality of predictions is constrained by input data resolution; higher-resolution DEMs and rainfall records would improve precision. Second, GAN training carries risks such as mode collapse, where diversity in synthetic samples may be lost. More advanced architectures (e.g., WGAN-GP) may mitigate this. Third, the study was restricted to Malang Regency; transferability of the trained model to other regions remains an open question. Fourth, the computational cost is nontrivial: ~25 minutes were required for GAN training and ~40 minutes for RBFN grid search on a Google Colab T4 GPU. While manageable for research, this cost may be restrictive for institutions with limited resources. Finally, this approach has important practical implications. By rehabilitating a model class previously unsuitable for imbalanced geospatial data, the GAN-RBFN pipeline expands the range of tools available for landslide susceptibility modeling. This flexibility opens pathways for tailoring models to specific data characteristics, improving hazard mapping, and ultimately supporting more informed spatial planning and risk mitigation strategies.

5. Conclusion

This research successfully demonstrated that severe data imbalance, specifically a 1:10 ratio, renders standard machine learning models like the KNN and RBFN ineffective for landslide prediction, with the RBFN failing entirely to identify any landslide events. However, the proposed integrated approach, which combines a GAN for data augmentation with a systematically tuned RBFN, proved to be a highly effective solution. This methodology dramatically improved the model's ability to detect landslides, elevating its performance from complete failure to a level comparable with the robust Random Forest benchmark. The primary contribution of this work is therefore the validation of a high-impact methodology for using GANs to optimize neural network classifiers in the context of imbalanced geospatial hazard data, effectively turning previously unreliable models into powerful predictive tools. This has significant practical implications, as it can lead to the development of more reliable and accurate landslide susceptibility maps, which are crucial for effective disaster mitigation, informed spatial planning, and the enhancement of early warning systems in vulnerable regions like East Java.

Building on these promising results, several avenues for future research are recommended to further advance this work. First, the generalizability and spatial transferability of the methodology should be rigorously tested by applying it to other geographical regions with different environmental characteristics and to adjacent, data-scarce areas. Second, further improvements to the augmentation process itself could be explored by investigating different and more advanced GAN architectures, such as Wasserstein GANs (WGAN-GP) or Conditional Tabular GANs (CTGAN), to potentially enhance the diversity and quality of the synthetic data. Finally, the practical utility of the model could be expanded by integrating dynamic, real-time data, such as daily or weekly rainfall, to transition from a static susceptibility map to a more dynamic, operational landslide forecasting system.

6. Declarations

6.1. Author Contributions

Conceptualization: C.R.A.W., I.M., Y.P., and A.M.W.; Methodology: I.M.; Software: C.R.A.W.; Validation: C.R.A.W., I.M., Y.P., and A.M.W.; Formal Analysis: C.R.A.W., I.M., Y.P., and A.M.W.; Investigation: C.R.A.W.; Resources: I.M.; Data Curation: I.M.; Writing Original Draft Preparation: C.R.A.W., I.M., Y.P., and A.M.W.; Writing Review and Editing: I.M., C.R.A.W., Y.P., and A.M.W.; Visualization: C.R.A.W.; All authors have read and agreed to the published version of the manuscript.

6.2. Data Availability Statement

The data presented in this study are available on request from the corresponding author.

6.3. Funding

The authors gratefully acknowledge the financial support for this research from the Fundamental Research Grant program of the Directorate General of Research and Development, Ministry of Higher Education, Science, and Technology of the Republic of Indonesia, for the fiscal year 2025. The authors also wish to express their gratitude to the Institute for Research and Community Service (LPPM) of Universitas Amikom Purwokerto for their institutional support and encouragement throughout this research. We would also like to extend our sincere gratitude to the various institutions that provided the data essential for this study. Special thanks are given to the Regional Disaster Management Agency (BPBD) of Malang Regency for providing the historical landslide inventory data. We also acknowledge the Geospatial Information Agency (BIG) for making the DEMNAS and Rupabumi Indonesia (RBI) data publicly accessible. This research would not have been possible without their support and the open availability of these crucial datasets.

6.4. Institutional Review Board Statement

Not applicable.

6.5. Informed Consent Statement

Not applicable.

6.6. Declaration of Competing Interest

The authors declare that they have no known competing financial interests or personal relationships that could have appeared to influence the work reported in this paper.

References

[1] N. Nurwatik, M. H. Ummah, A. B. Cahyono, M. R. Darminto, and J.-H. Hong, "A Comparison Study of Landslide Susceptibility Spatial Modeling Using Machine Learning," *ISPRS International Journal of Geo-Information,* vol. 11, no. 12, Art. no. 12, pp. 1-12, Dec. 2022, doi: 10.3390/ijgi11120602.

[2] I. Maulita, S. Sugito, and L. S. P. Boli, "Spatiotemporal Analysis of B-Value at Mount Slamet (2014–2023)," Jurnal Fisika Flux: Jurnal Ilmiah Fisika FMIPA Universitas Lambung Mangkurat, vol. 21, no. 3, pp. 255–268, Jan. 2025, doi: 10.20527/flux.v21i3.20718.

[3] M. Hürlimann, Z. Guo, C. P. i. Polo, and V. Medina, "Impacts of Future Climate and Land Cover Changes on Landslide Susceptibility: Regional Scale Modelling in the Val D'Aran Region (Pyrenees, Spain)," *Landslides*, vol. 19, no. 1, pp. 99–118, 2021, doi: 10.1007/s10346-021-01775-6.

[4] Z. Zou et al., "A novel method to evaluate the time-dependent stability of reservoir landslides: exemplified by Outang landslide in the Three Gorges Reservoir," *Landslides*, vol. 20, no. 8, pp. 1731–1746, Aug. 2023, doi: 10.1007/s10346-023-02056-0.

[5] Y. Pei et al., "Elevation dependence of landslide activity induced by climate change in the eastern Pamirs," *Landslides*, vol. 20, no. 6, pp. 1115–1133, June 2023, doi: 10.1007/s10346-023-02030-w.

[6] A. Wubalem, "Modeling of Landslide Susceptibility in a Part of Abay Basin, Northwestern Ethiopia," *Open Geosciences,* vol. 12, no. 1, pp. 1440–1467, 2020, doi: 10.1515/geo-2020-0206.

[7] S. K. Gupta and D. P. Shukla, "Handling data imbalance in machine learning based landslide susceptibility mapping: a case study of Mandakini River Basin, North-Western Himalayas," *Landslides*, vol. 20, no. 5, pp. 933–949, May 2023, doi: 10.1007/s10346-022-01998-1.

[8] J. R. Araújo, A. M. Ramos, P. M. M. Soares, R. Melo, S. C. Oliveira, and R. M. Trigo, "Impact of Extreme Rainfall Events on Landslide Activity in Portugal Under Climate Change Scenarios," *Landslides*, vol. 19, no. 10, pp. 2279–2293, 2022, doi: 10.1007/s10346-022-01895-7.

[9] A. L. Achu, S. Joseph, C. D. Aju, and J. Mathai, "Preliminary analysis of a catastrophic landslide event on 6 August 2020 at Pettimudi, Kerala State, India," *Landslides*, vol. 18, no. 4, pp. 1459–1463, Apr. 2021, doi: 10.1007/s10346-020-01598-x.

[10] L. Zhao, H. Ma, J. Dong, X. Wu, H. Xu, and R. Niu, "A Comparative Study of Landslide Susceptibility Mapping Using Bagging PU Learning in Class-Prior Probability Shift Datasets," *Remote Sensing*, vol. 15, no. 23, pp. 1-17, 2023, doi: 10.3390/rs15235547.

[11] Binh Thai Pham, Trung Nguyen-Thoi, Chongchong Qi, Tran Van Phong, Jie Dou, Lanh Si Ho, Hiep Van Le, and Indra Prakash, "Coupling RBF Neural Network With Ensemble Learning Techniques for Landslide Susceptibility Mapping," *Catena*, vol. 195, no. 1, pp. 1-12,, 2020, doi: 10.1016/j.catena.2020.104805.

[12] L. Yang and B. Li, "The Combination Forecasting Model of Grain Production Based on Stepwise Regression Method and RBF Neural Network," *Advance Journal of Food Science and Technology*, vol. 7, no. 11, pp. 891–895, 2015, doi: 10.19026/ajfst.7.2528.

[13] M. S. G. Adnan, M. S. Rahman, N. Ahmed, B. Ahmed, Md. F. Rabbi, and R. M. Rahman, "Improving Spatial Agreement in Machine Learning-Based Landslide Susceptibility Mapping," *Remote Sensing*, vol. 12, no. 20, pp. 1-12, 2020, doi: 10.3390/rs12203347.

[14] D. W. Apriani, C. Credidi, and S. Khala, "An Empirical-Statistical Model for Landslide Runout Distance Prediction in Indonesia," *Pondasi*, vol. 27, no. 1, pp. 15-26, 2022, doi: 10.30659/pondasi.v27i1.22618.

[15] M. Di Napoli, F. Carotenuto, A. Cevasco, P. Confuorto, D. Di Martire, M. Firpo, G. Pepe, E. Raso, and D. Calcaterra, "Machine learning ensemble modelling as a tool to improve landslide susceptibility mapping reliability," *Landslides*, vol. 17, no. 8, pp. 1897–1914, Aug. 2020, doi: 10.1007/s10346-020-01392-9.

[16] Y. Wang, X. Wu, Z. Chen, F. Ren, L. Feng, and Q. Du, "Optimizing the Predictive Ability of Machine Learning Methods for Landslide Susceptibility Mapping Using SMOTE for Lishui City in Zhejiang Province, China," *International Journal of Environmental Research and Public Health*, vol. 16, no. 3, pp. 1-12, 2019, doi: 10.3390/ijerph16030368.

[17] S. F. Pratama and A. M. Wahid, "Fraudulent Transaction Detection in Online Systems Using Random Forest and Gradient Boosting," *Journal of Cyber Law*, vol. 1, no. 1, pp. 88–115, Mar. 2025, doi: 10.63913/jcl.v1i1.5.

[18] Q. Siddique and A. M. Wahid, "Analyzing Customer Spending Based on Transactional Data Using the Random Forest Algorithm," *International Journal for Applied Information Management*, vol. 5, no. 2, pp. 111-124, May 2025, doi: 10.47738/ijaim.v5i2.103.

[19] M. A. Albahar, A. Alharbi, M. S. Alsuwat, and H. Aljuaid, "A Hybrid Model Based on Radial Basis Function Neural Network for Intrusion Detection," *International Journal of Advanced Computer Science and Applications*, vol. 11, no. 8, pp. 305-312, 2020, doi: 10.14569/ijacsa.2020.0110896.

[20] S. R. Meena, L. P. Soares, C. H. Grohmann, C. J. van Westen, K. Bhuyan, R. P. Singh, M. Floris, and F. Catani, "Landslide Detection in the Himalayas Using Machine Learning Algorithms and U-Net," *Landslides*, vol. 19, no. 5, pp. 1209–1229, 2022, doi: 10.1007/s10346-022-01861-3.

[21] C. R. Ajeng Widiawati, H. Adi Nugroho, I. Ardiyanto, and M. S. Amin, "Increasing Performance of Plasmodium Detection Using Bottom-Hat and Adaptive Thresholding," in *2021 IEEE 5th International Conference on Information Technology, Information Systems and Electrical Engineering (ICITISEE)*, vol. 2021, no. Nov., pp. 207–212, 2021. doi: 10.1109/ICITISEE53823.2021.9655903.

[22] A. M. Wahid, T. Hariguna, and G. Karyono, "Optimization of Recommender Systems for Image-Based Website Themes Using Transfer Learning," *Journal of Applied Data Sciences*, vol. 6, no. 2, Art. no. 2, pp. 1-12, Mar. 2025, doi: 10.47738/jads.v6i2.671.

[23] A. Ageenko, L. C. Hansen, K. L. Lyng, L. Bodum, and J. J. Arsanjani, "Landslide Susceptibility Mapping Using Machine Learning: A Danish Case Study," *Isprs International Journal of Geo-Information*, vol. 11, no. 6, pp. 324-338, 2022, doi: 10.3390/ijgi11060324.